Check for updates

The enhancement of reactive red 24 adsorption from aqueous solution using agricultural waste-derived biochar modified with ZnO nanoparticles

Huu Tap Van, [iD] *[a] Lan Huong Nguyen,[b] N. V. Dang, [iD] *[c] Huan-Ping Chao,[d] Quang Trung Nguyen,[a] Thu Huong Nguyen,[a] Thi Bich Lien Nguyen,[a] Dang Van Thanh,[e] Hai Duy Nguyen,[f] Phan Quang Thang,[g] Pham Thi Ha Thanh[h] and Vinh Phu Hoang[i]

In this study, two types of agricultural wastes, sugarcane bagasse (SB) and cassava root husks (CRHs), were used to fabricate biochars. The pristine biochars derived from SB and CRHs (SBB and CRHB, respectively) were modified using ZnO nanoparticles to generate modified biochars (SBB-ZnO and CRHB-ZnO, respectively) for the removal of Reactive Red 24 (RR24) from stimulated wastewater. Batch experiments were performed to evaluate the effects of ZnO nanoparticles' loading ratio, solution pH, contact time, and initial RR24 concentration on the RR24 adsorption capacity of biochars. The RR24 adsorption isotherm and kinetic data on SBB, SBB-ZnO3, CRHB, and CRHB-ZnO3 were analyzed. Results indicate that SB- and CRH-derived biochars with a ZnO nanoparticle loading ratio of 3 wt% could generate maximum adsorption capacities of RR24 thanks to the double growth on the BET surface of modified biochars. The RR24 adsorption capacities of CRHB-ZnO3 and SBB-ZnO3 reached 81.04 and 105.24 mg g^{-1}, respectively, which were much higher than those of pristine CRHB and SBB (66.19 and 76.14, respectively) at an initial RR24 concentration of 250 mg L^{-1}, pH 3, and contact time of 60 min. The adsorption of RR24 onto biochars agreed well with the pseudo-first-order model and the Langmuir isotherm. The RR24 adsorption capacity on modified biochars, which were reused after five adsorption–desorption cycles showed no insignificant drop. The main adsorption mechanisms of RR24 onto biochars were controlled by electrostatic interactions between biochars' surface positively charged functional groups with azo dye anions, pore filling, hydrogen bonding formation, and π–π interaction.

1. Introduction

Reactive dyes are widely used in industries, such as rubber, paper, leather, plastics, and textile.[1,2] Typically, approximately

[a]*Faculty of Natural Resources and Environment, TNU – University of Sciences (TNUS), Tan Thinh Ward, Thai Nguyen City 24000, Vietnam. E-mail: tapvh@tnus.edu.vn*

[b]*Faculty of Environment – Natural Resources and Climate Change, Ho Chi Minh City University of Food Industry (HUFI), Ho Chi Minh City, Vietnam*

[c]*Faculty of Physics and Technology, TNU – University of Sciences (TNUS), Tan Thinh Ward, Thai Nguyen City, Vietnam. E-mail: dangnv@tnus.edu.vn*

[d]*Department of Environmental Engineering, Chung Yuan Christian University, Taoyuan 32023, Taiwan*

[e]*TNU – University of Medicine and Pharmacy, Thai Nguyen, Vietnam*

[f]*Faculty of Environment, Thai Nguyen University of Agriculture and Forestry (TUAF), Thai Nguyen City 24000, Vietnam*

[g]*Institute of Environmental Technology, Vietnam Academy of Science and Technology, 18 Hoang Quoc Viet Road, Ha Noi City, Vietnam*

[h]*Faculty of Chemistry, TNU – University of Education, No. 20, Luong Ngoc Quyen Road, Thai Nguyen City, Vietnam*

[i]*School of Chemistry, Biology and Environment, Vinh University, No. 182 Le Duan, Vinh City, Nghe An Province, Vietnam*

40% of residual reactive dyes from the textile industry is released into the environment.[1] Owing to the poor fixation, non-degradability, and toxicity properties as well as potential carcinogenicity,[3] mutagenicity, and teratogenicity,[4] reactive dyes can cause serious impacts to the human health and aquatic ecosystem. In particular, several azo dyes can be incompletely degraded or transformed into harmful aromatic amines in the presence of anoxic sediments.[5] Therefore, residual azo dyes from industrial wastewater effluents need to be removed before being discharged into receiving bodies to protect the environment and human health.

Several methods comprising biological treatment, chemical and electrochemical coagulation, membrane separation, and advanced oxidation can effectively treat dyes.[6,7] The biological method could partly remove azo dyes from wastewater with low cost and environment friendliness but high risk to microbial life due to their toxicity.[8] On the other hand, physical and chemical methods prove effective in the treatment of dyes.[9] Among physicochemical treatment methods, adsorption is considered an effective method for the removal of azo dyes compared with the other methods because of its relatively low

operation cost, high treatment efficiency, non-toxicity, and in particular, it was suitable for the removal of the residue from the secondary effluent. Recently, a wide range of adsorbents have been applied in the treatment of azo dyes, consisting of zeolites,[10] activated carbon,[11] biochar,[12] fly ash,[13] magnetic graphene oxide/chitosan composites,[14] and nanoparticles.[15,16] Among adsorbents, biochars generated from agricultural wastes have widely been used to remove different pollutants. For example, bael shell (*Aegle marmelos*)-derived biochar was used for the treatment of patent blue dye[17] and corncob-derived biochar was employed for the removal of ammonia from simulated wastewater.[18]

Out of agricultural wastes, cassava root husks (CRHs) and sugarcane bagasse (SB) have been widely used to produce biochars as low-cost non-toxic adsorbents for the removal of various pollutants from wastewater. In particular, carbon materials have a high surface area with a large pore volume and modified materials possess more oxygen-containing functional groups, which enhance H bonding and $\pi-\pi$ interaction between biochar and the aromatic ring contaminants.[19] For instance, cassava residue-derived biochars were used to remove methylene blue,[20] Cd,[21] and malachite green[22] from aqueous solutions, whereas SB-derived biochars were applied to adsorb pollutants such as Congo red,[23] benzidine, *o*-toluidine,[24] and phosphorus[25] from wastewaters. However, these CRHs and SB derived-pristine biochars required a long adsorption time with a limited surface area and a badly-developed pore structure and gave low adsorption capacity toward macromolecules such as azo dyes, which is not conducive for application in practice. Therefore, a number of investigators intended to modify the CRH- and SB-derived biochars (CRHB and SBB, respectively) by various methods. At present, SBB has been modified by aluminum sulfate for the removal of industrial cutting fluid[26] and Pb^{2+} ions,[27] while Mg has been employed for the treatment of ammonium and phosphate ions[28] and TiO$_2$ nanoparticle-loaded SBB for the adsorption of methylene blue[29] to improve its adsorption efficiency, whereas the studies regarding the use of CRHBs for the removal of pollutants are quite scarce. In particular, research about the modification of both CRHB and SBB by loading ZnO nanoparticles for the removal of azo dyes from aqueous solutions have not been found in the literature.

Moreover, cassava and sugarcane are the most popular agricultural plants in Asia and Vietnam. Annually, large amounts of CRHs and SB are generated, leading to difficulties in solid waste management and treatment. Hence, the utilization of these wastes to fabricate biochars, then their modification by loading ZnO nanoparticles to obtain effective adsorbents for the enhancement of contaminant removal from aqueous solution should be of interest.

In this study, to enhance the RR24 adsorption efficiency and capacity onto the biochars, the ZnO nanoparticles were chosen to fully load onto the biochars' surface. The reason for this was because the ZnO nanoparticles possess a high surface area, low-cost, non-toxicity, and high chemical stability.[30–32] Furthermore, there were some scholars that have reported to use biochar derived from various materials, which were impregnated in ZnO nanoparticles to improve the adsorption capacity of different

pollutants from wastewater. The reports indicated that in comparison with pristine biochars, the biochars modified by nanoparticles exhibited excellent higher adsorption capacity towards various pollutants in wastewater.[33,34] Hence, the present work chose ZnO nanoparticles to load on the cassava root husks (CRHs) and sugarcane bagasse (SB) derived-pristine biochars for the adsorption of RR24 from aqueous solution.

The findings in this study showed that the generation of ZnO-modified biochars derived from agricultural wastes is a new, suitable, and feasible approach to treat persistent organic pollutants in wastewater.

To achieve this goal, batch adsorption experiments were conducted using modified biochars under different operational conditions to investigate the effects of the loading ratio of ZnO nanoparticles, the solution pH, contact time, adsorbent dosage, and initial RR24 concentration on the RR24 adsorption capacity onto the biochars. The characteristics of biochars, which comprised textural, morphology properties, and surface chemistry were systematically analyzed. Also, the RR24 adsorption isotherm and kinetics for adsorption on the biochars were investigated to elucidate the adsorption mechanisms of RR24 onto the ZnO nanoparticle-modified biochars.

The obtained results can be used to evaluate the potential of application of ZnO nanoparticle-modified biochars for the adsorption of azo dyes from wastewater with a new, low-cost, and highly effective adsorbent.

2. Materials and methods

2.1. Materials

RR24 (Tianjin, China) was selected as the target azo dye in this study. Other chemicals, including ZnO, H$_2$SO$_4$, NaOH, and high-purity (>99%) Zn metal rods were purchased from Merck (Germany). Simulated azo dye wastewater was prepared in the laboratory *via* the dissolution of RR24 in distilled water. CRHs and SB were collected from Quyet Thang ward, Thai Nguyen City, Vietnam.

2.2. Synthesis of ZnO nanoparticles

ZnO nanoparticles were synthesized using an electrochemical method.[35] A 0.5 M KCl solution was used as the electrolyte. Two Zn metal rods were prepared to be the electrodes. The electrochemical system was placed in a cooling water bath at 30–50 °C and operated at a working voltage of 10 V. The ZnO nanoparticles were generated using a TES-6220 (Centenary Materials Co., Ltd., Taiwan) regulated direct-current power supply. The system was stirred at 400 rpm using an IKA® C-MAG HS 4 (IKA, France) magnetic stirrer. The obtained milky-white suspension of ZnO nanoparticles after 60 min of stirring was cooled to 25 ± 2 °C. Afterwards, the collected ZnO nanoparticles were filtered through a polyvinylidene difluoride membrane with a pore size of 0.2 μm, followed by drying at 80 °C for 12 h. Finally, the ZnO nanoparticles were stored in plastic bags for further use.

2.3. Preparation of biochars

For the fabrication of pristine biochars, CRHs and SB were firstly washed with tap water, followed by drying at 105 °C in an

Paper

RSC Advances

oven. In the next step, the dried CRHs and SB were crushed into small pieces of size 1–2 cm. Subsequently, these CRHs and SB pieces were heated under a pyrolysis temperature of 400 °C in a L3/11/B170 (Nabertherm, Germany) furnace under oxygen-limited conditions with a heating rate of 30 °C min^{-1} for 2 h. Thereafter, the products were sieved to obtain biochar particles with size less than 0.5 mm and the obtained cassava root husks biochar (CRHB) and sugarcane bagasse biochar (SBB) samples were stored in plastic bags for further use.

For the fabrication of modified biochars, an incipient wet-impregnation method followed by heating at 100 °C was used to load ZnO nanoparticles onto pristine CRHB and SBB. The above obtained ZnO nanoparticles were added into 250 mL Erlenmeyer flasks, which contained a certain amount of CRHB or SBB and distilled water. The loading ratio of ZnO onto biochars ranged between 1 and 5 wt%. The mixtures were subsequently stirred for 30 min at 25 ± 2 °C to obtain the biochars, which was contained in the suspensions. In the next step, the suspensions were heated at 100 °C for 4 h. Finally, the suspensions were filtered and dried at 105 °C for 2 h to obtain the modified biochars. The obtained modified biochars were labelled as CRHB-ZnO and SBB-ZnO. The ZnO-modified CRHB and SBB samples at the ZnO nanoparticle loading ratio of 1, 3, and 5 wt%, respectively, were termed as CRHB-ZnO1, CRHB-ZnO3, CRHB-ZnO5 and SBB-ZnO1, SBB-ZnO3, SBB-ZnO5. All the modified biochar samples were stored in plastic bags and were subsequently used for conducting RR24 adsorption experiments.

2.4. Characteristics of biochars

The pore volume and surface area of the biochars before and after RR24 adsorption were determined by the Brunauer–Emmett–Teller (BET) method using an SA 3000 (Coulter, USA) instrument. The surface functional groups of the adsorbents were identified using a FTIR-6300 (Manufacturer, Country) Fourier-transform infrared spectrometer (FTIR) in the wavenumber range of 4000–500 cm^{-1}. An S-4800 (Hitachi, Japan) scanning electron microscope (SEM) equipped with an energy-dispersive electron spectrometer (EDS) was used to evaluate the shape and surface morphology of the adsorbents. The point of zero charge (pH$_{PZC}$) was obtained from the abscissa intercept of the ΔpH $vs.$ pH$_i$ curve.[36] The X-ray photoelectron spectroscopy (XPS) profiles of the biochars were obtained using an ESCALAB 250 (Thermo Scientific, US) instrument with an Al Kα X-ray source (1486.6 eV).

2.5. Adsorption experiments

All batch adsorption experiments of RR24 onto CRHB, SBB, CRHB-ZnO, and SBB-ZnO were performed in 50 mL Erlenmeyer flasks at room temperature (25 ± 2 °C).

To determine the optimal ZnO nanoparticle loading ratio, 1.0 g L^{-1} of each adsorbent (SBB, SBB-ZnO1, SBB-ZnO3, SBB-ZnO5, CRHB, CRHB-ZnO1, CRHB-ZnO3, and CRHB-ZnO5) and 25 mL of the 200 mg L^{-1} RR24 solution were separately supplemented into each 50 mL Erlenmeyer flask. The flasks were then shaken at 120 rpm using a PH-4A shaker (STECH,

China) for 120 min at pH 4. The effect of the solution pH in the range of 3–10 on RR24 adsorption by biochars was performed at an initial RR24 concentration of 200 mg L^{-1}, adsorbent dose of 1.0 g L^{-1}, and contact time of 60 min.

The experiments aimed to study RR24 adsorption kinetic onto CRHB, SBB and CRHB-ZnO, SBB-ZnO (at the optimal loading ratio of ZnO nanoparticles) were conducted by varying the contact time in the range of 5–120 min with fixed experimental conditions at the above obtained optimal pH value at an initial RR24 concentration of 200 mg L^{-1} and adsorbent dose of 1.0 g L^{-1}.

In addition, the RR24 adsorption isothermal experiments onto CRHB, SBB, CRHB-ZnO, and SBB-ZnO were also conducted by varying the initial RR24 concentrations in the range of 25–350 mg L^{-1} with the optimal parameters determined in the above experiments with an adsorbent dosage of 1.0 g L^{-1}. The samples collected at regular intervals during the experiment process were filtered through 0.45 μm filters. The remaining RR24 concentration in the filtrates was determined by the colorimetric method at the wavelength of 534 nm using a Z2000 (Shimadzu, Japan) UV-Vis spectrophotometer.[6]

2.6. Regeneration and reusability experiments

For regeneration experiments, as soon as the CRHB-ZnO3 and SBB-ZnO3 adsorbent samples were saturated with RR24 particles, and the biochars were filtered and separated from the aqueous solutions. In the next step, a dosage of 0.2 g of CRHB-ZnO3 or SBB-ZnO3 was separately soaked in 50 mL of 1 M NaOH solution for 24 h at 25 ± 2 °C. Thereafter, the samples were dried at 105 °C before being reused for the adsorption experiments. Each biochar sample was subjected to five adsorption–desorption cycles and aliquots were collected at certain intervals to determine the RR24 adsorption capacities onto the biochars.

The reusability experiments were performed in the batch mode at an initial RR24 concentration of 200 mg L^{-1}, adsorbent dose of 1.0 g L^{-1}, solution pH of 3, and contact time of 60 min at room temperature (25 ± 2 °C) using adsorbents that were regenerated in the above experiments.

2.7. Calculation

The adsorption capacities at time t (q_t, mg g^{-1}) and equilibrium (q_e, mg g^{-1}) were calculated as follows.

$$q_e = \frac{(C_o - C_e)V}{W} \tag{1}$$

and

$$q_t = \frac{(C_o - C_t)V}{W}, \tag{2}$$

where, C_o (mg L^{-1}) is the initial RR24 concentration, C_t (mg L^{-1}) and C_e (mg L^{-1}) are the RR24 concentrations at time t and equilibrium, respectively, V (L) is the working volume of the RR24 solution, and W (g) is the mass of the adsorbent used for each experiment.

All the experiments were conducted in two parallel samples at the same time. The data were analyzed using MS Excel and Origin 9.0 software. The data were presented as mean ± standard deviation.

3. Results and discussion

3.1. Effect of ZnO nanoparticle loading ratio on RR24 adsorption by the biochars

The effect of ZnO nanoparticle loading ratio on RR24 adsorption by SBB, SBB-ZnO1, SBB-ZnO3, SBB-ZnO5, CRHB, CRHB-ZnO1, CRHB-ZnO3, and CRHB-ZnO5 are presented in Fig. 1. In general, it is significant from the data in Fig. 1 that the adsorption capacities of SBB-ZnO and CRHB-ZnO for RR24 were higher than those of pristine SBB and CRHB, respectively, owing to the presence of ZnO nanoparticles on the surfaces of SBB-ZnO and CRHB-ZnO. Moreover, the RR24 adsorption capacities of SBB-ZnO and CRHB-ZnO increased as the ZnO nanoparticle loading ratio increased from 1 to 3 wt% (Fig. 1). However, the RR24 adsorption capacities of both CRHB-ZnO and SBB-ZnO decreased slightly when the ZnO nanoparticle loading ratio increased from 3 to 5 wt%. This was ascribed to the decrease in the surface areas of SBB-ZnO and CRHB-ZnO when the ZnO nanoparticle loading ratio exceeded 3 wt%, which caused a drop in their adsorption capacities for RR24. This trend was similar to that of the previously reported studies.[37–39] For instance, Nguyen *et al.* (2019)[38] indicated that the Cr(VI) adsorption capacity of Ag nanoparticle-modified activated carbon increased with the Ag nanoparticle loading ratio and reached a plateau at a loading ratio of 2 wt%. Trinh *et al.* (2020)[37] reported that the optimal Ag nanoparticle loading for the adsorption of P was 3 wt%. Also, the RR24 adsorption capacities of SBB and SBB-ZnO were not significantly higher than those of CRHB and CRHB-ZnO. Furthermore, SBB-ZnO3 and CRHB-ZnO3 showed the highest adsorption capacities for RR24 (Fig. 1). After 90 min of adsorption time, the RR24 adsorption capacities of SBB and SBB-ZnO3 were 72.94 and 92.93 mg g^{-1}, respectively, and these values for CRHB and CRHB-ZnO3 were 66.74 and 84.15 mg g^{-1}, respectively. This

could be attributed to the surface areas and pore volumes of SBB and SBB-ZnO3, which were higher than those of CRHB and CRHB-ZnO3, respectively (Table 1). Hence, the optimum ZnO nanoparticle loading ratio of the modified biochars was determined to be 3 wt%, and SBB-ZnO3 and CRHB-ZnO3 were used for the subsequent experiments.

3.2. Physical properties of the adsorbents

The physical properties of SBB, SBB-ZnO3, CRHB, and CRHB-ZnO3 are summarized in Table 1. From Table 1, it can be seen that both the surface area and pore volume of SBB-ZnO3 and CRHB-ZnO3 were higher than those of pristine SBB and CRHB. Clearly, the surface areas of the modified biochars were about two times higher than that of pristine biochars. Significantly, after the modification of ZnO-NPs, the pore volumes of SBB and CRHB changed from 0.0079 and 0.0011 cm^3 g^{-1} to 0.0124 and 0.0069 cm^3 g^{-1}, respectively, and the surface area of SBB and CRHB changed from 2.1043 and 1.9056 m^2 g^{-1} to 4.0703 and 2.3831 m^2 g^{-1}, respectively. Although the modification of pristine biochars enhanced the BET surface area and pore volume of the biochars, these biochars still possessed a low surface area and pore volume. The physical properties of both pristine and modified biochars followed the increasing order CRHB < SBB < CRHB-ZnO3 < SBB-ZnO3 for the BET surface area and pore volume (Table 1). On the basis of the analysis and discussion regarding the BET surface area and pore volume data of the biochars, it is clearly that the contribution of the pore-filling mechanism in RR24 adsorption onto the biochars was negligible. The BET surface area and pore volume of the biochars, which were applied in this study, were similar to some other biochars such as cassava rind carbon,[22] iron-modified biochar from corncob,[39] and eucalyptus bark bio-char.[12]

3.3. Effect of solution pH

The solution pH strongly affects the surface charge of the biochars and the charge of the dye ions in solution. In this study, the effect of the solution pH in the range of 3–10 on RR24 adsorption by CRHB, SBB, CRHB-ZnO3, and SBB-ZnO3 at an
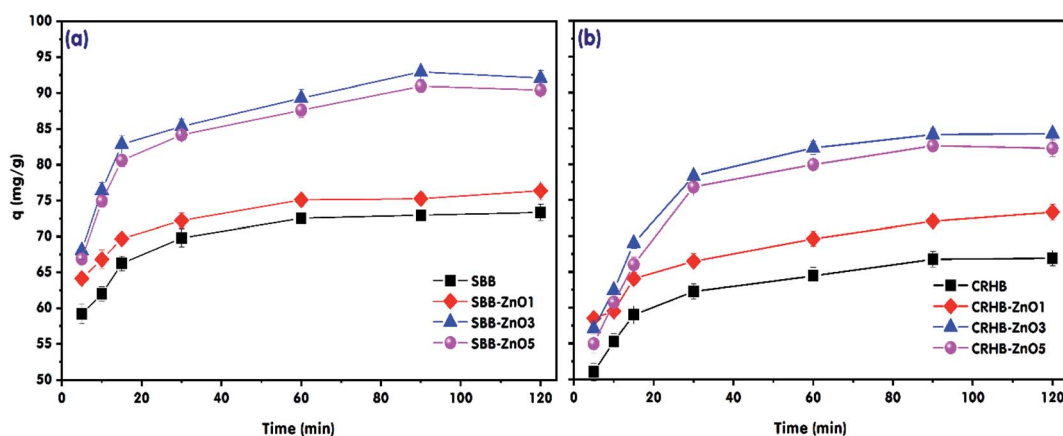

Fig. 1 Effect of ZnO nanoparticle loading ratio on the RR24 adsorption capacities (q) of (a) SBB and (b) CRHB at the experimental conditions: initial RR24 concentration of 200 mg L^{-1}, adsorbent dose of 1.0 g L^{-1}, pH of 4, room temperature (25 ± 2 °C).

Table 1 Physical properties of both pristine and modified biochars

Biochar	S_{BET} (m^2 g^{-1})	Pore volume (cm^3 g^{-1})	Biochar	S_{BET} (m^2 g^{-1})	Pore volume (cm^3 g^{-1})
SBB	2.1043	0.0079	Cassava rind carbon[22]	2.38	0.565
SBB-ZnO3	4.0703	0.0124	Iron modified biochar from corncob[39]	1.49	0.0031
CRHB	1.9056	0.0011	Eucalyptus bark bio-char[12]	0.56	
CRHB-ZnO3	2.3831	0.0069			

absorbent dosage of 1.0 g L^{-1} with an initial RR24 concentration of 200 mg L^{-1} and contact time of 60 min at a temperature of 25 ± 2 °C was investigated. The obtained results are illustrated in Fig. 2a. It can be seen from Fig. 2a that the RR24 adsorption capacities of CRHB, SBB, CRHB-ZnO3, and SBB-ZnO3 witnessed a slight fall when the solution pH increased from 3 to 10. The maximum adsorption capacities of CRHB, CRHB-ZnO3, SBB, and SBB-ZnO3 for RR24 reached 72.55, 86.36, 73.31, and 97.82 mg g^{-1}, respectively, at pH 3. Besides, the RR24 adsorption capacities of CRHB-ZnO3 and SBB-ZnO3 were higher than those of pristine CRHB and SBB, and the RR24 adsorption capacities of SBB and SBB-ZnO3 were slightly higher than those of CRHB and CRHB-ZnO3, respectively, over the entire studied pH range. The pH$_{PZC}$ value plays a crucial role in the selection of the optimal pH for adsorption studies and for further ascertaining the adsorption mechanism. The pH$_{PZC}$ values of CRHB, CRHB-ZnO3, SBB, and SBB-ZnO3 were determined to be 8.25, 6.94, 6.60, and 6.69, respectively (Fig. 2b). When pH$_{PZC}$ is higher than the solution pH, the surfaces of the biochars became predominantly positively charged and the RR24 molecules were ionized in the aqueous solution (eqn (3)) and became negatively charged owing to the presence of sulfate groups.

$$Dye–SO_3Na \rightarrow dye–SO_3^- + Na^+ \qquad (3)$$
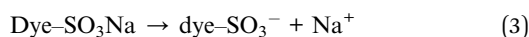
Therefore, at low pH levels, the high adsorption capacities of the biochars for RR24 were attributed to the chemical adsorption, which was dominated by the electrostatic interaction

between the positively charged functional groups on the surfaces of the biochars and dye–SO$_3^-$ anions.[3,4] Moreover, in the aforementioned experiments, at a solution pH of 3, the RR24 adsorption capacities of CRHB and CRHB-ZnO3 were marginally lower than those of SBB and SBB-ZnO3. This might be ascribed to the higher pH$_{PZC}$ values of CRHB and CRHB-ZnO3 than those of SBB and SBB-ZnO3 (Fig. 2b). Nonetheless, the RR24 adsorption capacities of the aforementioned adsorbents saw a moderate downward trend at higher solution pH levels. These results were due to the competition between the dye–SO$_3^-$ and OH$^-$ anions in solution, which resulted in a reduction in the intensity of the interactions between the dye–SO$_3^-$ anions and positively charged ions on the surface of the biochars.[17] Besides, the electrostatic repulsive forces could have occurred between the dye–SO$_3^-$ anions and positively charged ions on the surfaces of the biochars.[4] The fall in the adsorption capacities of the adsorbents for anionic dyes when raising the solution pH from acidic to alkaline was similar to that in the other studies.[2,3,17] Therefore, it can be concluded that a pH 3 was optimal for the adsorption of RR24 onto SBB-ZnO3 and CRHB-ZnO3, and the electrostatic attraction was the main mechanism for RR24 adsorption onto the biochars. Besides, there was also the contribution of pore filling, π–π interaction, and hydrogen bonding formation mechanisms in the adsorption process of RR24 onto the biochars.[40,41]

3.4. Effect of the contact time and adsorption kinetic study

The effect of the contact time towards RR24 adsorption onto various biochars was investigated and the results are presented in Fig. 3. The experiments were conducted at an initial RR24
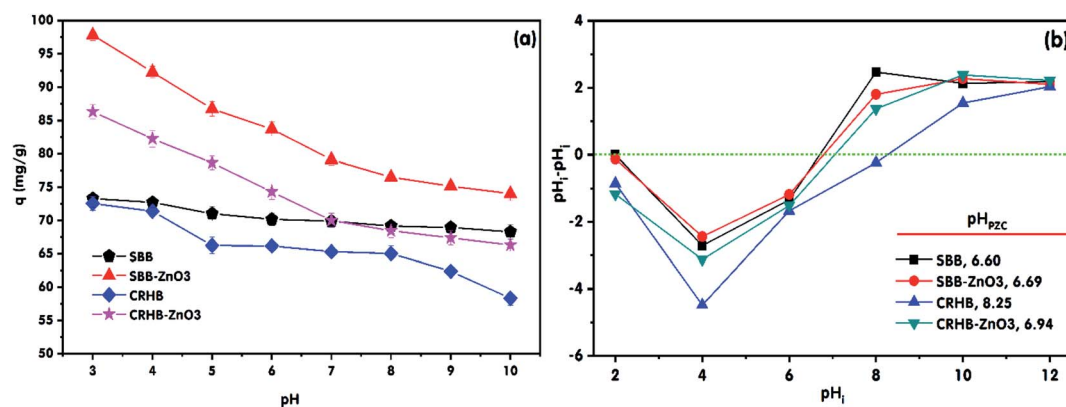

Fig. 2 Effect of the solution pH on the (a) RR24 adsorption onto various biochars and (b) pH$_{PZC}$ value of the biochars at experimental conditions: initial RR24 concentration of 200 mg L^{-1}, adsorbent dose of 1.0 g L^{-1}, and the contact time of 60 min at room temperature (25 ± 2 °C).
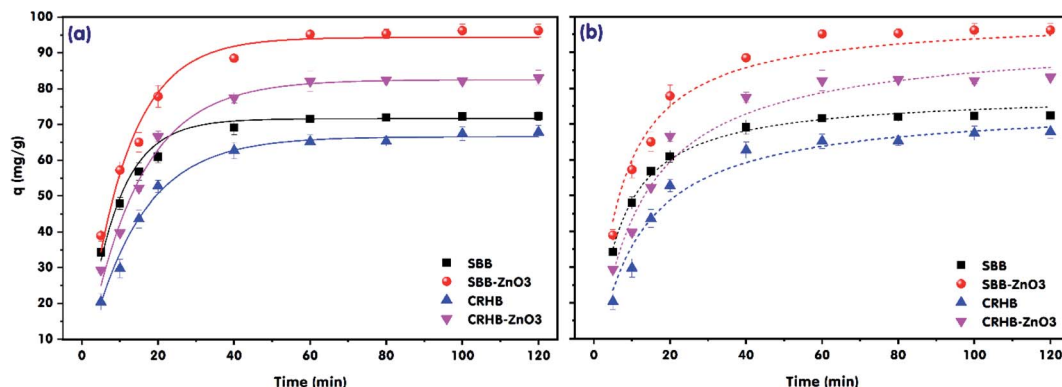
Fig. 3 Effects of contact time and RR24 adsorption kinetics onto different biochars: (a) pseudo-first-order and (b) pseudo-second-order model at experimental conditions: contact time of 120 min, initial RR24 concentration of 200 mg L^{-1}, adsorbent dose of 1.0 g L^{-1}, and pH of 3.

concentration of 200 mg L^{-1}, solution pH of 3.0, and adsorbent dose of 1.0 g L^{-1} with varying contact time in the range from 5 to 120 min. As can be seen from Fig. 3, the RR24 adsorption capacities of CRHB, CRHB-ZnO3, SBB, and SBB-ZnO3 increased during the first 20 min of contact and this trend was gradually slowed down by a slight growth during 40–60 min of contact. The adsorption capacities of almost all the adsorbents reached plateaus after approximately 60 min. The highest adsorption capacities of CRHB, CRHB-ZnO3, SBB, and SBB-ZnO3 for RR24 after 60 min of contact time were 65.18, 82.12, 71.57, and 95.13 mg g^{-1}, respectively. The increase in the RR24 adsorption capacities of the adsorbents during the initial contact stage could be attributed to the large number of available active sites on the surface of the adsorbents, causing a growth in the attraction between the dye ions and the adsorbent surfaces. The high initial adsorption rate revealed that the adsorbents presented strong affinity towards the target azo dye anions. The kinetic studies play an important role in scaling the reactor volume up to apply and to ensure the efficiency and economy in pollutant removal in practice.

In this study, the pseudo-first-order (PFO)[42] and pseudo-second-order (PSO)[43] kinetic models were used to describe the adsorption dynamics of RR24 onto the biochars. The non-linearized forms of the PFO and PSO kinetic models can be expressed as follows.

$$q_t = q_e(1 - e^{-k_1 t}) \quad (4)$$

and

$$q_t = \frac{q_e^2 k_2 t}{1 + k_2 q_e t}, \quad (5)$$

where, k_1 (min^{-1}) and k_2 (g (mg^{-1} min^{-1})) are the rate constants of the PFO and PSO kinetic models, respectively. The prediction curves of the models and kinetic parameters for RR24 adsorption are presented in Fig. 3 and Table 1, respectively.

Table 2 illustrates the correlation coefficients (R^2) of RR24 adsorption onto CRHB, CRHB-ZnO3, SBB, and SBB-ZnO3 after fitting the experimental data using the PFO and PSO models. The R^2 values were close to 1.0. In addition, the q_e values

calculated using the PFO ($q_{e,cal} = 66.57$–94.31 mg g^{-1}) and PSO ($q_{e,cal} = 65.51$–98.01 mg g^{-1}) kinetic models were in good agreement with the experimental values ($q_{e,exp} = 65.18$–95.13 mg g^{-1}). Consequently, both the PFO and PSO models well-described RR24 adsorption onto CRHB, CRHB-ZnO3, SBB, and SBB-ZnO3. However, the $q_{e,cal}$ calculated values using the PFO model were closer to the $q_{e,exp}$ data. These results demonstrate that the PFO model could be used to describe the adsorption of RR24 on the biochars more effectively than on the PSO model. Furthermore, these results indicate that the adsorption of RR24 onto the biochars was dominated by valence forces *via* the sharing of electrons between the dye anions and cations on the adsorbent surface.[44] The closing $q_{e,cal}$ and $q_{e,exp}$ values obtained using the PFO and PSO models suggest that the rate-limiting step for the adsorption process was chemisorption, originating from the bidentate type bridge between the SO_3^- anions of RR24 and the adsorbents,[45] which caused the modified biochars combined with RR24 by chemical attraction to have stable physicochemical characteristic and thus have no secondary pollution effects on the environment. Similar adsorption mechanisms of the azo dyes have been previously reported, including the adsorption of Remazol Black 5 and Remazol Brilliant Orange 3R onto glutaraldehyde-crosslinked chitosans;[44] the adsorption of azo dye Orange II onto iron-

Table 2 Calculated kinetic parameters of RR24 adsorption onto pristine and modified biochars

	Adsorbent			
	SBB	SBB-ZnO3	CRHB	CRHB-ZnO3
Pseudo-first order model				
q_e (mg g^{-1})	71.63	94.31	66.57	82.54
k_1 (g (mg^{-1} min^{-1}))	0.1179	0.0907	0.0716	0.0718
R^2	0.9884	0.9778	0.9878	0.9892
Pseudo-second order model				
q_e (mg g^{-1})	78.61	98.01	65.51	84.28
k_2 (min^{-1})	0.0021	0.0015	0.0012	0.0015
R^2	0.9909	0.9609	0.9629	0.9769

benzene tricarboxylate[7] and the adsorption of Congo red onto porous CeO_2 nanotubes.[45]

3.5. Effect of the initial RR24 concentration and adsorption isotherm study

The effects of the initial RR24 concentration on the RR24 adsorption capacities onto CRHB, CRHB-ZnO3, SBB, and SBB-ZnO3 and the adsorption isotherms are indicated in Fig. 4. The experimental conditions were set up at a solution pH of 3.0, adsorbent dosage of 1.0 g L^{-1}, and contact time of 60 min with varying initial RR24 concentration in the range of 25–350 mg L^{-1}. Overall, it is significant from the data in Fig. 4 that the RR24 adsorption capacities of all the used adsorbents gradually rose with increasing initial RR24 concentration from 25 to 350 mg L^{-1} and reached plateaus at an RR24 initial concentration of 250 mg L^{-1}. More azo dye anions were transformed from the aqueous solution to the surfaces of CRHB, CRHB-ZnO3, SBB, and SBB-ZnO3 via the available binding sites. Moreover, with the same adsorbent dosage and solution volume, the number of available binding sites was high when the initial concentration of RR24 was low (<250 mg L^{-1})[7] and became limited when the initial concentration of RR24 was high (>250 mg L^{-1}).[46] In this study, the maximum adsorption capacities of RR24 onto CRHB, CRHB-ZnO3, SBB, and SBB-ZnO3 at the initial RR24 concentration of 250 mg L^{-1} were 66.19, 81.04, 76.14, and 105.24 mg g^{-1}, respectively. Besides, the adsorption capacities of RR24 onto CRHB-ZnO3 and SBB-ZnO3 exceeded those of pristine CRHB and SBB by 14.08 and 29.10 mg g^{-1}, and the adsorption capacities of SBB and SBB-ZnO3 were

higher than those of CRHB and CRHB-ZnO3, respectively. These results confirmed that the RR24 adsorption capacities onto CRHB, CRHB-ZnO3, SBB, and SBB-ZnO3 strongly depended on the initial RR24 concentration. As a result, the RR24 adsorption capacities of the applied adsorbents followed the increasing order CRHB < SBB < CRHB-ZnO3 < SBB-ZnO3.

To further elucidate the adsorption mechanism of RR24 onto CRHB, CRHB-ZnO3, SBB, and SBB-ZnO3, the Langmuir,[47] Freundlich,[48] and Sips[49] models were applied (eqn (6), (7), and (8), respectively) to fit the experimental data.

$$q_e = \frac{q_m b C_e}{1 + b C_e}, \tag{6}$$

$$q_e = K_F C_e^{1/n}, \tag{7}$$

and

$$q_e = \frac{q_m (b C_e)^{1/n}}{1 + (b C_e)^{1/n}}, \tag{8}$$

where, C_e is the equilibrium concentration of RR24 (mg L^{-1}), b (L mg^{-1}) is the Langmuir constant related to the free adsorption energy, K_L (L mg^{-1}) and K_F (mg g^{-1}) are the Langmuir and Freundlich constants, respectively, and n is the adsorption intensity.

The calculated K_F, K_L, and R^2 values for the three models are presented in Table 3 and the plots are illustrated in Fig. 4. It is significant from the data in Table 3 and Fig. 4 that all the calculated R^2 values were higher than 0.95, which confirmed that the aforementioned models fitted the experimental data
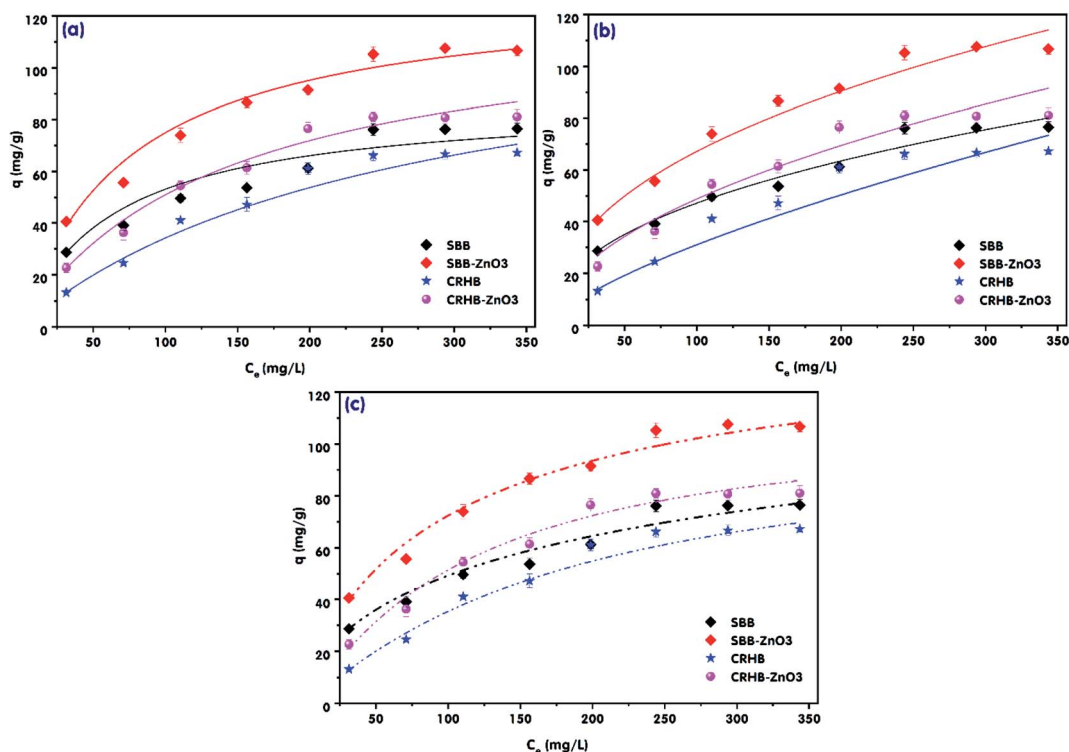

Fig. 4 RR24 adsorption isotherms onto the biochars: (a) Langmuir model; (b) Freundlich model, and (c) Sips model.

Table 3 Calculated isotherm parameters and correlation coefficients (R^2) of RR24 adsorption isotherm models onto the biochars

Model	Adsorbents			
	SBB	SBB-ZnO3	CRHB	CRHB-ZnO3
Langmuir				
$q_{e,cal}$ (mg g^{-1})	77.41	110.36	64.71	82.15
K_L (L mg^{-1})	0.0155	0.0135	0.0038	0.0007
R^2	0.9975	0.9925	0.9972	0.9996
Freundlich				
K_F (mg g^{-1}) (mg L^{-1})^n	6.5452	9.2968	1.2510	4.6569
n	2.3315	2.3288	1.4342	1.9605
R^2	0.9947	0.9902	0.9697	0.9497
Sips				
$q_{e,cal}$ (mg g^{-1})	80.64	107.07	63.54	79.66
b	0.0272	0.0209	0.0030	0.0048
n	1.5931	1.2114	0.8950	0.8862
R^2	0.9912	0.9895	0.9887	0.9808

very well for RR24 adsorption onto CRHB, CRHB-ZnO3, SBB, and SBB-ZnO3 (Table 3). However, the experimental data fitted the Langmuir model ($R^2 > 0.99$) better than the Sips ($R^2 = 0.9808–0.9912$) and Freundlich models ($R^2 = 0.9697–0.9947$). The $q_{e,cal}$ values for CRHB, CRHB-ZnO3, SBB, and SBB-ZnO3 ranged between 64.71–110.36 mg g^{-1} (Langmuir model) and 80.64–107.07 (Sips model). Furthermore, in this study, K_L ranged between 0.0007–0.0135. These values were lower than unity, which indicated that adsorption was favorable.[7] Besides, the n values of the Freundlich model was in the range of 1.434–2.332, which was higher than that of the Sips model (0.8862–1.5931), confirmed that RR24 adsorption onto CRHB, CRHB-ZnO3, SBB, and SBB-ZnO3 was favorable.[50] The $q_{e,cal}$ values of CRHB, CRHB-ZnO3, SBB, and SBB-ZnO3 reached 64.71, 82.15, 74.11, and 101.36 mg g^{-1} for the Langmuir model and 63.54, 79.66, 80.64, and 107.07 for the Sips model, respectively, and the corresponding $q_{e,exp}$ values were 66.19, 81.04, 76.14, and 105.24 mg g^{-1}. To summarize, it can be concluded from the results summarized in Fig. 4 and Table 3 that the Langmuir model was the most suitable for describing the RR24 adsorption kinetics onto CRHB, CRHB-ZnO3, SBB, and SBB-ZnO3. These findings demonstrated that RR24 adsorption onto the biochars occurred *via* monolayer adsorption onto a homogeneous

surface. The analogue results have been reported for the adsorption of anionic azo dyes onto different absorbents, such as graphene oxide,[51] fly ash-iron oxide magnetic nano-composites,[10] and gasification wood residue-derived biochar.[52]

In this study, to confirm the feasibility of the biochars for the removal of dyes from textile industry effluents, the RR24 adsorption capacity onto various biochars was compared with those of several adsorbents for the removal of different azo dyes reported in previous studies and the results are summarized in Table 4. From Table 4, it can be seen that to date, no studies have focused on the use of CRHB-ZnO and SBB-ZnO for the removal of RR24 from aqueous solutions. The maximum adsorption capacities (q_{max}) of CRHB-ZnO and SBB-ZnO for RR24 were higher than those of many other adsorbents, comprising wheat straw biochar for the removal of methylene blue dye[53] and magnetic zeolite/iron oxide nanocomposite for the removal of reactive orange 16.[10] Meanwhile, the adsorption capacities of the adsorbents in this study were similar to that of magnetic cobalt-iron oxide nanoparticles (CoFeNPs1/ CoFeNPs2) for the removal of reactive orange 16.[15] However, several adsorbents have presented higher RR24 adsorption capacities than those of the biochars in this study, namely, CuFe$_2$O$_4$/activated carbon for the adsorption of acid orange 7,[54] *Eucalyptus sheathiana* bark biochar for the removal of methylene blue dye,[12] and Zr-based chitosan for the adsorption of Orange II.[4] The optimal solution pH for RR24 adsorption in this study was similar to those for the adsorption of various azo dyes reported in ref. 15, where CoFeNPs1/CoFeNPs2 was used for the removal of reactive orange 16, and in ref. 4, where Zr-based chitosan was utilized for the removal of Orange II. These comparison results demonstrate that CRHB-ZnO and SBB-ZnO are feasible, low-cost, and highly effective for the removal of azo dyes from wastewater.

3.6. Reusability of CRHB-ZnO3 and SBB-ZnO3

Owing to economic and environmental reasons, the reusability of adsorbents is a crucial factor for practical applications. Therefore, the reusability of CRHB-ZnO3 and SBB-ZnO3 for RR24 adsorption was studied using 1.0 M NaOH solution with the following experimental conditions: initial concentration of RR24 200 mg L^{-1}, adsorbent dose 1.0 g L^{-1}, solution pH of 3, room temperature (25 ± 2 °C), and contact time of 60 min. High concentration of NaOH was selected for the desorption

Table 4 Comparison of adsorption of azo dyes onto various adsorbents

| Azo dye	Adsorbent	pH	Time (min)	q_{max} (mg g^{-1})	References
Acid orange 7	CuFe$_2$O$_4$/activated carbon	5.2	1140	392	54
Reactive orange 16	CoFeNPs1/CoFeNPs2	4	75	68	15
Methylene blue	Magnetic zeolite/iron oxide nanocomposite	10	40	1.1	10
	Eucalyptus sheathiana bark biochar	11.3	150	104.2	12
	Wheat straw biochar	8–9	120	12.03	53
Orange II	Zr-based chitosan	2	30	926	4
Reactive red 24	CRHB-ZnO3	3	60	71.13	This study
	SBB-ZnO3	3	60	75.13	This study
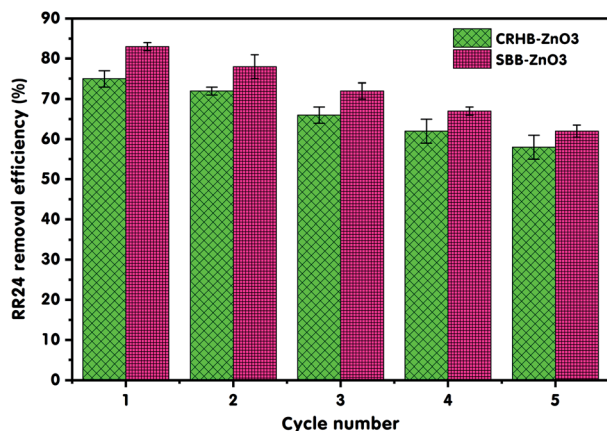
Fig. 5 Reusability of modified biochars for the removal of RR24 through five adsorption–desorption cycles.

experiments because almost RR24 ions were released into the solution at high pH.[4] The reusability of both CRHB-ZnO3 and SBB-ZnO3 for RR24 adsorption over five cycles is presented in Fig. 5. After five cycles of reuse, the adsorption efficiencies of

SBB-ZnO3 and CRHB-ZnO3 desorbed by NaOH decreased from 85.28% to 62.84% and from 75.32% to 58.22%, respectively (Fig. 5). However, the RR24 adsorption efficiencies onto modified biochars still exceed 50% but were higher than those of pristine SBB and CRHB. The decrease in the adsorption efficiencies of the desorbed biochars through adsorption–desorption cycles was because of the loss of functional groups and incomplete desorption.[55] These reusability results indicate that CRHB-ZnO3 and SBB-ZnO3 are promising adsorbents for the removal of azo dyes from aqueous solutions and real wastewaters with excellent reusability and stability.

3.7. Characteristic of biochars and the adsorption mechanism

Fig. 6 and 7 illustrate the SEM images and energy-dispersive X-ray spectroscopy (EDS) profiles of SBB, SBB-ZnO3, CRHB, and CRHB-ZnO3 before and after the adsorption of RR24. All the biochars indicated very rough and heterogamous surface structures before (Fig. 6a, b, 7a, and b) and after (Fig. 6c and 7c) adsorption. The SEM images and EDS profiles of the biochars further revealed that SBB-ZnO3 and CRHB-ZnO3 presented
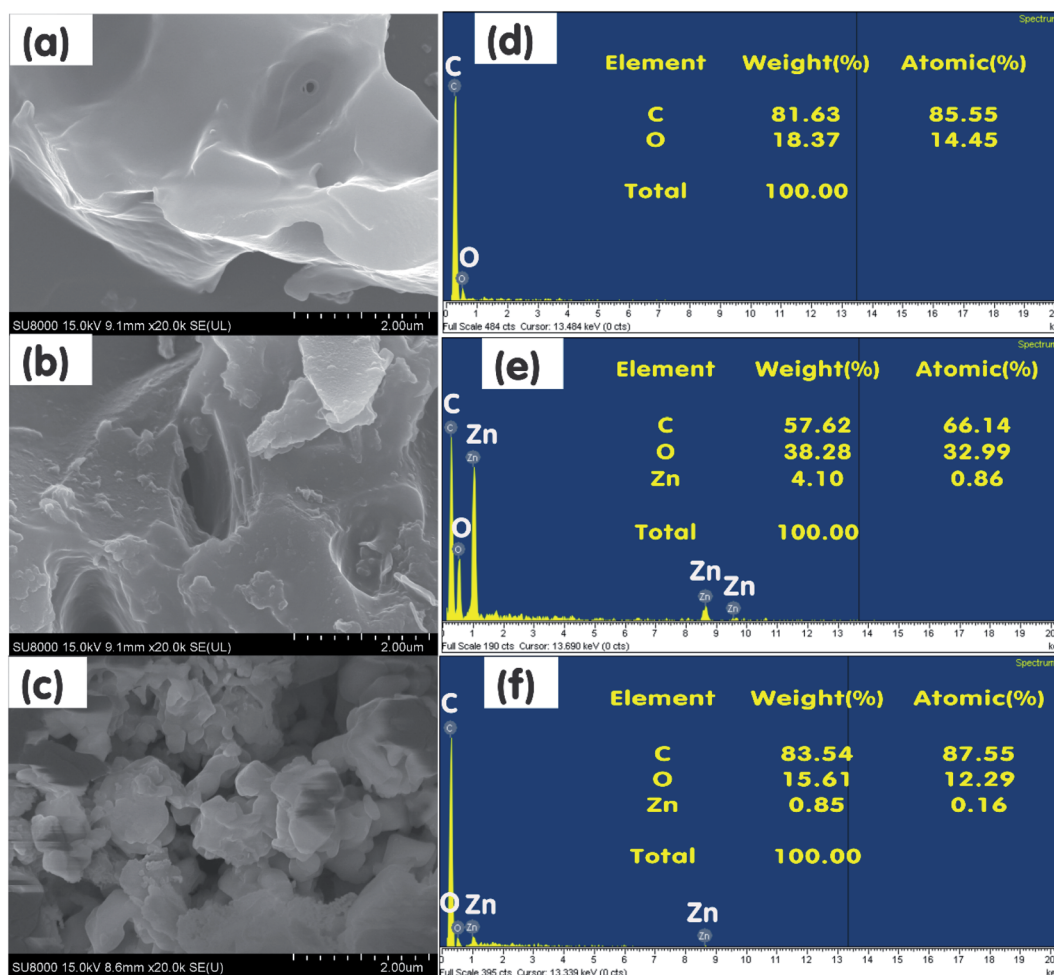

Fig. 6 SEM of (a) pristine SBB and (b) SBB-ZnO3 before and (c) SBB-ZnO3 after RR24 adsorption; EDX of (d) pristine SBB and (e) SBB-ZnO3 before and (f) SBB-ZnO3 after RR24 adsorption.

more porous and rougher structures than those of pristine SBB and CRHB.

The results of EDS analysis indicated that the constituents of SBB, SBB-ZnO3 before, and SBB-ZnO3 after RR24 adsorption mostly consisted of C (81.63%, 57.62%, and 83.54%, respectively) and O (18.37%, 38.28%, and 15.61%, respectively) (Fig. 6d–f). In addition, the Zn content of SBB-ZnO3 before and after the adsorption of RR24 were 4.10% and 0.85%, respectively. The O content of SBB-ZnO3 before RR24 adsorption was higher than that of pristine SBB, which demonstrated that ZnO nanoparticles were successfully loaded onto the surface of SBB.

Similarly, the constituents of pristine CRHB, CRHB-ZnO3 before, and CRHB-ZnO3 after RR24 adsorption mostly consisted of C and O elements (Fig. 7d–f). However, CRHB and CRHB-ZnO3 also contained Al, Si, K, Ca, and Fe. The presence of Zn in CRHB-ZnO3 before and after the adsorption of RR24 further confirmed that the ZnO nanoparticles were successfully loaded onto the surface of CRHB.

Clearly, the ZnO-modified biochars before the adsorption of RR24 developed quite a good pore structure and surface area, leading to more sites for the adsorption of RR24. After the adsorption of RR24, the pore structure on the biochars' surface

disappeared, which proved that RR24 were partly adsorbed onto the biochars through the pore filling mechanism.[41]

The analysis of FTIR spectra of SBB, SBB-ZnO3, CRHB, and CRHB-ZnO3 in Fig. 8 shows that the oxygen-containing main functional groups on the surface of the biochars before and after RR24 adsorption were C–H, C–O, C=C, C=O, and –OH. The peak associated with the stretching vibration of the –OH groups was observed at 3651 cm^{-1} in the FTIR spectra of SBB, SBB-ZnO3 before, and after RR24 adsorption (Fig. 8a) at 3873 cm^{-1} in the FTIR spectra of CRHB and CRHB-ZnO3 before the adsorption of RR24, and at 3749 cm^{-1} in the FTIR spectrum of CRHB-ZnO3 after the adsorption of RR24. The peaks in the range of 3500–3900 cm^{-1} confirmed the presence of –OH groups in the structures of SBB, SBB-ZnO3, CRHB, and CRHB-ZnO3.[56] The peaks in the ranges of 520–876 cm^{-1} in CRHB and CRHB-ZnO3 before and after RR24 adsorption (Fig. 8b) and 553–767 cm^{-1} in SBB and SBB-ZnO3 before and after RR24 adsorption of RR24 (Fig. 8a) suggested the presence of C–H groups in the structures of these adsorbents.[39] Furthermore, the peak at 750 cm^{-1} in the spectrum of CRHB-ZnO3 before the adsorption of RR24 shifted to 720 cm^{-1} in the spectrum of CRHB-ZnO3 after the adsorption of RR24. The peaks of the C–O
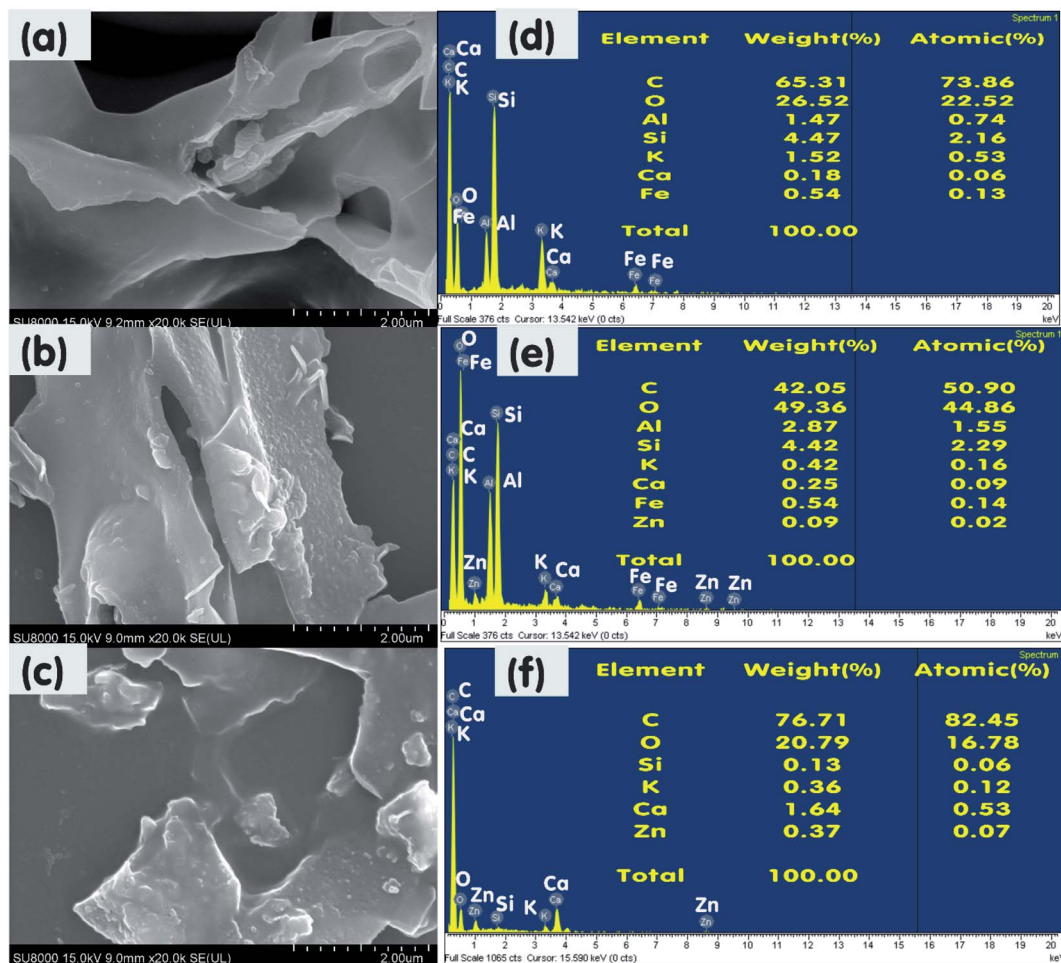

Fig. 7 SEM of (a) pristine CRHB and (b) CRHB-ZnO3 before and (c) CRHB-ZnO3 after RR24 adsorption; and EDX of (d) pristine CRHB and (e) CRHB-ZnO3 before and (f) CRHB-ZnO3 after RR24 adsorption.
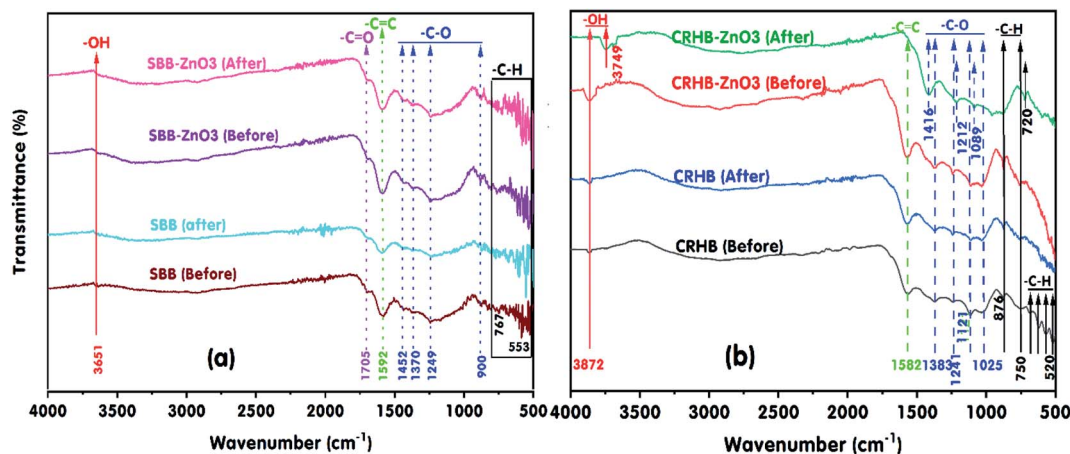
Fig. 8 FTIR of pristine SBB and SBB-ZnO3 before and after RR24 adsorption (a) and (b) pristine CRHB and CRHB-ZnO3 before and after RR24 adsorption.

groups were observed at 900, 1249, 1370, and 1452 cm^{-1} in the FTIR spectra of SBB and SBB-ZnO3 before and after RR24 adsorption and at 1025, 1089, 1121, 1241, and 1383 cm^{-1} in the FTIR spectra of both CRHB and CRHB-ZnO3 before and after the adsorption of RR24.[29] The peaks associated with the C=C groups were observed in the wavenumber range of 2349–2520 cm^{-1} in the FTIR spectra of both CRHB and CRHB-ZnO3 before and after RR24 adsorption.[27] Furthermore, the peaks at 1121, 1241, and 1383 cm^{-1} in the FTIR spectrum of CRHB-ZnO3 before RR24 adsorption shifted to 1089, 1212, and 1416 cm^{-1}, respectively, in the FTIR spectrum of CRHB-ZnO3 after the adsorption of RR24. The peaks of the C=C groups represented the characteristic peak of benzene ring or the aromatic ring, which was observed at 1592 cm^{-1} (SBB, SBB-ZnO3 before, and SBB-ZnO3 after RR24 adsorption) and 1582 cm^{-1} (CRHB, CRHB-ZnO3 before, and CRHB-ZnO3 after the adsorption of RR24). Besides, the peak of the C=O group was identified at 1705 cm^{-1} (SBB, SBB-ZnO3 before, and SBB-ZnO3 after RR24 adsorption).[27] These oxygen-containing functional groups acted as π-electron acceptors during the adsorption process.[57] The loading of ZnO nanoparticles onto the biochars during the carbonization process resulted in the aromatization of the carbon skeleton.[58] Moreover, RR24 are organic compounds and contain unsaturated bonds. In this study, the formed biochars at the pyrolysis temperature of 400 °C had aromatic ring structures, which enhanced the π–π interaction thanks to the C=C and C=O bonds on the biochars' surface (Fig. 8). The formation of π–π interaction was due to the aromatic rings of the RR24 molecules, which acted as π-electron acceptors and the aromatic ring structure of the modified biochars (*i.e.*, C–O–C and C=O) acted as π-electron donors.[41] Thus, π–π interaction was regarded as a potential adsorption mechanism for the adsorption of RR24 onto the modified biochars. Besides, hydrogen bonding occurred between the phenolic group of RR24 and the oxygen-containing groups on the biochars' surface (*i.e.*, –COOH or –OH),[59] leading to the enhancement of RR24 adsorption onto the biochars.

The surface charge measurements revealed that the pH$_{PZC}$ values of SBB, SBB-ZnO3, CRHB, and CRHB-ZnO3 were 6.60, 6.69, 8.25, and 6.69, respectively, which were higher than that of solution pH, leading to the biochars' surface predominantly positive charge due to the deprotonation of oxygen-containing surface groups. Therefore, the electrostatic attraction between the dye–SO$_3^-$ anions and positively charged adsorption sites of SBB, SBB-ZnO3, CRHB, and CRHB-ZnO3 increased, which corresponded to the increase in the RR24 adsorption capacities of the biochars at a solution pH of 3. In this study, the data analysis of the adsorption isotherms and kinetic further demonstrated that adsorption was mainly controlled by the electrostatic interactions between RR24 and the biochars. Moreover, the functional groups on the surfaces of SBB, SBB-ZnO3, CRHB, and CRHB-ZnO3 played an important role in RR24 adsorption. In addition, Zn^{4+} ions could be formed *via* the protonation of the Zn atoms on the surfaces of SBB-ZnO3 and CRHB-ZnO3 at low pH levels. Therefore, electrostatic interactions could have occurred between the Zn^{4+} cations and dye–SO$_3^-$ anions.[4] On the other hand, the dye removal mechanism was predicted by functional groups using FTIR spectroscopy. The FTIR spectra of SBB-ZnO3 and CRHB-ZnO3 before and after RR24 adsorption are depicted in Fig. 8. The peaks ascribed to the –OH, C–H, and C–O groups shifted significantly after the adsorption of RR24, probably owing to the strong interactions between SBB-ZnO3 or CRHB-ZnO3 and RR24, from which it can be concluded that the aromatic group joined in the whole adsorption process.

The RR24 adsorption capacity of SBB-ZnO3 was the highest in all the samples owing to the BET surface area and pore volume of SBB-ZnO3 being higher than those of SBB, CRHB, and CRHB-ZnO3 (Table 1). The ZnO nanoparticles were easily loaded on the biochar with a high surface area and pore volume. Besides, the presence of Zn element on the surfaces of CRHB-ZnO3 and SBB-ZnO3 demonstrated the successful loading of ZnO nanoparticles onto pristine CRHB and SBB (Fig. 6 and 7, respectively). Furthermore, the adsorption capacities of SBB-ZnO3 and CRHB-ZnO3 were higher than those of pristine SBB
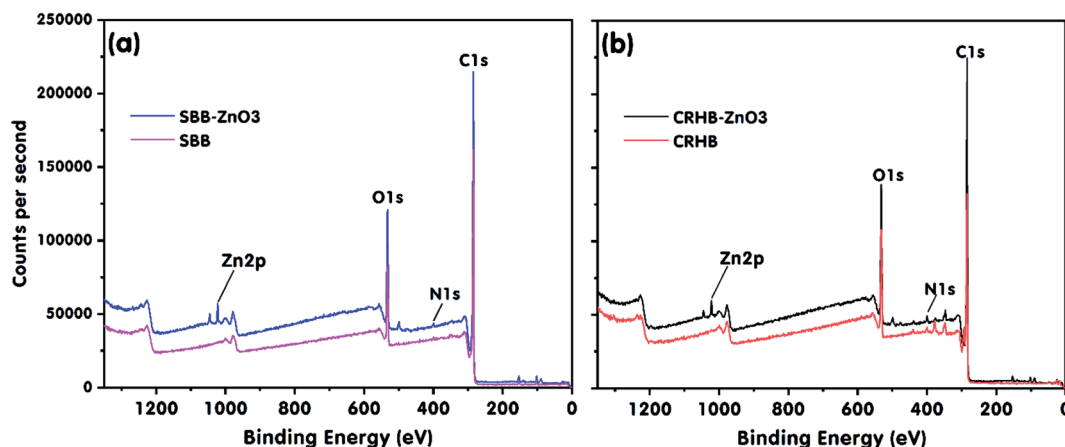
Fig. 9 XPS of (a) pristine SBB and SBB-ZnO3 and (b) pristine CRHB and CRHB-ZnO3.

and CRHB, respectively. This suggested that ZnO played an important role in RR24 adsorption onto SBB-ZnO3 and CRHB-ZnO3 by a noticeable growth in the high surface area of the modified biochars. The EDS results (Fig. 6e and 7e) indicated that the amount of Zn loaded on SBB-ZnO3 was higher than that of CRHB-ZnO3. Despite the appearance of several other elements (Ca, K, Fe, Al, and Si) on the surface of CRHB-ZnO3, the RR24 adsorption capacity of SBB-ZnO3 was also higher than that of CRHB-ZnO3. This indicated that ZnO nanoparticles on the surfaces of the biochars were the main factor that enhanced RR24 removal from the aqueous solutions. It can be explained that ZnO nanoparticles acted as both the adsorbents and photocatalysts for the degradation of RR24.[60] Therefore, the adsorption capacity of SBB-ZnO3 was higher than those of SBB, CRHB, and CRHB-ZnO3 thanks to the highest amount of Zn present in SBB-ZnO3 (Fig. 6e and 7e).

The XPS results in Fig. 9 revealed the changes in the structures and valences of the elements present on the surfaces of SBB, SBB-ZnO3, CRHB, and CRHB-ZnO3. The Zn 2p peaks were observed at 1022.19 and 1021.86 eV in the XPS profiles of SBB-ZnO3 and CRHB-ZnO3, respectively. This further confirmed that the ZnO nanoparticles were successfully loaded onto these biochars and the important role of ZnO in RR24 adsorption onto SBB-ZnO3 and CRHB-ZnO3.

Furthermore, the surface chemistry and proportion of oxygen-carrying chemical functional groups on the surface of the biochars were detected by XPS analysis (Fig. 9). A predominant peak at the binding energy (B.E.) of 284.52 eV corresponds to the aromatic rings and aliphatic structures (such as $-CH_x$, C–C, and C=C). The presence of oxygen-carrying functional groups was identified at three binding energies of 285.92 eV ($-C$–OR in alcohols or phenols), 286.34 eV (C=O in carbonyl, ketone, and quinone groups), and 287.49 eV (O–C=O in carboxyl groups). Moreover, the binding energy peak located at 289.7 eV was designated to the π–π* shake-up satellite peak because of the abundant presence of π-electrons in aromatic rings.[61–63] The results indicated that the ZnO modified biochars contained the oxygen-containing functional groups on the surface. The results were consistent with the FTIR data in Fig. 8.

Overall, the RR24 adsorption mechanisms onto the biochars mainly comprised electrostatic interaction, hydrogen bonding formation, and π–π interaction.

4. Conclusion

In this study, low-cost adsorbents derived from SB and CRHs were developed *via* pyrolysis. Subsequently, the obtained biochars were successfully modified by loading ZnO nanoparticles onto the biochars' surface using the electrochemical method. The ZnO-modified biochars exposed high adsorption capacities toward RR24 from simulated wastewater. The ZnO nanoparticles that successfully attached onto the surface of the biochars remarkably enhanced the removal of RR24 by the modified biochars. The physical and chemical properties of all the biochars before and after the adsorption of RR24 were analyzed in detail using different methods. The optimal solution pH for the adsorption of RR24 onto CRHB, CRHB-ZnO3, SBB, and SBB-ZnO3 was 3. The results also indicated that the RR24 adsorption capacities of CRHB, CRHB-ZnO3, SBB, and SBB-ZnO3 increased with the increase in the contact time and the initial concentration of RR24. The maximum RR24 adsorption capacities of CRHB, CRHB-ZnO3, SBB, and SBB-ZnO3 were 66.19, 81.04, 76.14, and 105.24 mg g^{-1}, respectively, at an initial RR24 concentration of 250 mg L^{-1}, which were higher than those of the values previously reported in the literature. The experimental data for RR24 adsorption onto CRHB, CRHB-ZnO3, SBB, and SBB-ZnO3 fitted best with the Langmuir and PFO models. In addition, the data describing the characteristics of the adsorbents and studies of pH, pH_{PZC}, can ascertain that the main mechanism for RR24 adsorption onto the ZnO nanoparticle-modified biochars, including CRHB-ZnO3 and SBB-ZnO3, was electrostatic attraction, pore filling, H bonding formation, and π–π interaction. In particular, the regeneration experiments demonstrated that the RR24 removal efficiency of CRHB-ZnO3 and SBB-ZnO3 was remarkably unchanged after multiple adsorption–desorption cycles. Therefore, it can be concluded that all CRHB, CRHB-ZnO3, SBB, and SBB-ZnO3

can be potential low-cost and highly effective adsorbents for the removal of azo dyes from wastewater.

Conflicts of interest

The authors declare that they have no conflict of interest.

Acknowledgements

References

1 Z. Alimohammadi, H. Younesi and N. Bahramifar, *Waste Biomass Valorization*, 2016, **7**, 1255–1270.

2 X. Mi, Z. Shang, C. Du, G. Li, T. Su, X. Chang, R. Li, Z. Zheng and J. Tie, *J. Chem.*, 2018, 1–8.

3 S. Karmakar, D. Roy, C. Janiak and S. De, *Sep. Purif. Technol.*, 2019, **215**, 259–275.

4 L. Zhang, L. Chen, X. Liu and W. Zhang, *RSC Adv.*, 2015, **5**, 93840–93849.

5 B. Lellis, C. Z. Fávaro-Polonio, J. A. Pamphile and J. C. Polonio, *Biotechnol. Res. Innov.*, 2019, **3**, 275–290.

6 H. T. Van, L. H. Nguyen, T. K. Hoang, T. P. Tran, A. T. Vo, T. T. Pham and X. C. Nguyen, *Sep. Purif. Technol.*, 2019, **224**, 431–442.

7 E. R. García, R. L. Medina, M. M. Lozano, I. H. Pérez, M. J. Valero and A. M. Maubert Franco, *Materials*, 2014, **7**, 8037–8057.

8 J. Wu, H. Doan and S. Upreti, *Chem. Eng. J.*, 2008, **142**, 156–160.

9 S. Kong, W. Zhang, S. Gao and D. Chen, *J. Exp. Nanosci.*, 2019, **14**, 107–115.

10 D. A. Fungaro, *J. At. Mol. Sci.*, 2011, **2**, 305–316.

11 H. Albroomi, M. Elsayed, A. Baraka and M. Abdelmaged, *Int. Conf. Chem. Environ. Eng.*, 2014, vol. 7, pp. 1–13.

12 S. Dawood, T. K. Sen and C. Phan, *Desalin. Water Treat.*, 2016, **57**, 28964–28980.

13 G. Patra, R. Barnwal, S. K. Behera and B. C. Meikap, *J. Environ. Chem. Eng.*, 2018, **6**, 5204–5211.

14 T. T. N. Le, V. T. Le, M. U. Dao, Q. V. Nguyen, T. T. Vu, M. H. Nguyen, D. L. Tran and H. S. Le, *Chem. Eng. Commun.*, 2019, **206**, 1337–1352.

15 Qurrat-Ul-Ain, S. Khurshid, Z. Gul, J. Khatoon, M. R. Shah, I. Hamid, I. A. T. Khan and F. Aslam, *RSC Adv.*, 2019, **10**, 1021–1041.

16 T. P. M. Chu, N. T. Nguyen, T. L. Vu, T. H. Dao, L. C. Dinh, H. L. Nguyen, T. H. Hoang, T. S. Le and T. D. Pham, *Materials*, 2019, **12**, 1–15.

17 K. Roy, K. M. Verma, K. Vikrant, M. Goswami, R. K. Sonwani, B. N. Rai, K. Vellingiri, K. H. Kim, B. S. Giri and R. S. Singh, *Sustainability*, 2018, **10**, 2669–2681.

18 L. H. Nguyen, T. M. Vu, T. T. Le, V. T. Trinh, T. P. Tran and H. T. Van, *Environ. Technol.*, 2019, **40**, 683–692.

19 X. R. Jing, Y. Y. Wang, W. J. Liu, Y. K. Wang and H. Jiang, *Chem. Eng. J.*, 2014, **248**, 168–174.

20 A. J. Rubio, I. Z. Silva, F. Gasparotto, E. A. S. Paccola, C. N. Silva, I. P. Emanuelli, R. Bergamasco and N. U. Yamaguchi, *Chem. Eng. Trans.*, 2018, **65**, 751–756.

21 A. R. Bakhtiari, M. P. Zakaria, M. I. Yaziz, M. N. H. L. Lajis and X. Bi, *EnvironmentAsia*, 2014, **7**, 104–111.

22 B. H. Beakou, K. El Hassani, M. A. Houssaini, M. Belbahloul, E. Oukani and A. Anouar, *Water Sci. Technol.*, 2017, **76**, 1447–1456.

23 Z. Zhang, L. Moghaddam, I. M. O'Hara and W. O. S. Doherty, *Chem. Eng. J.*, 2011, **178**, 122–128.

24 M. R. M. Adib, M. H. M. N. Attahirah and A. R. M. Amirza, *IOP Conf. Ser. Earth Environ. Sci.*, 2018, **140**, 012029.

25 L. Fang, J. Shan Li, S. Donatello, C. R. Cheeseman, C. S. Poon and D. C. W. Tsang, *J. Cleaner Prod.*, 2020, **244**, 118853.

26 N. Pongtaveekan, P. Thammajaree, K. Piyamongkala, N. Pongstabodee and V. L. R. Manguiam, *J. Eng.*, 2019, 1–11.

27 Poonam, S. K. Bharti and N. Kumar, *Appl. Water Sci.*, 2018, **8**, 1–13.

28 M. E. Saleh and R. M. R. Hedia, *Alexandria Sci. Exch. J.*, 2018, **39**, 74–91.

29 R. A. El-Salamony, E. Amdeha, S. A. Ghoneim, N. A. Badawy, K. M. Salem and A. M. Al-Sabagh, *Environ. Technol.*, 2017, **38**, 3122–3136.

30 Z. L. Wang, *J. Phys.: Condens. Matter*, 2004, **16**, R829–R858.

31 L. Zhang, Y. Jiang, Y. Ding, M. Povey and D. York, *J. Nanopart. Res.*, 2007, **9**, 479–489.

32 Ü. Özgür, Y. Alivov, C. Liu, A. Teke, M. Reshchikov, S. Dogan, V. Avrutin, S.-J. Cho and H. Morkoç, *J. Appl. Phys.*, 2005, **98**, 41301.

33 C. Li, L. Zhang, Y. Gao and A. Li, *Waste Manage.*, 2018, **79**, 625–637.

34 M. Chen, C. Bao, D. Hu, X. Jin and Q. Huang, *J. Anal. Appl. Pyrolysis*, 2019, **139**, 319–332.

35 D. T. H. Phuong, D. Van Thanh, N. P. Chi, L. T. Quynh, N. X. Hoa, H. X. Linh and N. N. Huy, *J. Electron. Mater.*, 2020, **49**, 917–921.

36 G. M. D. Ferreira, G. M. D. Ferreira, M. C. Hespanhol, J. de Paula Rezende, A. C. dos Santos Pires, L. V. A. Gurgel and L. H. M. da Silva, *Colloids Surf., A*, 2017, **529**, 531–540.

37 V. T. Trinh, T. Minh, P. Nguyen, H. T. Van and L. P. Hoang, *Sci. Rep.*, 2020, **10**, 1–13.

38 L. H. Nguyen, T. M. P. Nguyen, H. T. Van, X. H. Vu, T. L. A. Ha, T. H. V. Nguyen, X. H. Nguyen and X. C. Nguyen, *Water, Air, Soil Pollut.*, 2019, **230**, 68–82.

39 L. P. Hoang, H. T. Van, L. H. Nguyen, D. H. Mac, T. T. Vu, L. T. Ha and X. C. Nguyen, *New J. Chem.*, 2019, **43**, 18663–18672.

40 H. M. Jang and E. Kan, *Bioresour. Technol.*, 2019, **284**, 437–447.

41 B. Wang, Y. s. Jiang, F. y. Li and D. y. Yang, *Bioresour. Technol.*, 2017, **233**, 159–165.

42 S. Lagergren, *Sven. Vetenskapsakad. Handingarl*, 1898, **24**, 1–39.

43 G. Blanchard, M. Maunaye and G. Martin, *Water Res.*, 1984, **18**, 1501–1507.

44 A. H. Chen and S. M. Chen, *J. Hazard. Mater.*, 2009, **172**, 1111–1121.

45 J. Wu, J. Wang, Y. Du, H. Li and X. Jia, *J. Nanopart. Res.*, 2016, **18**, 191–204.

46 N. A. Salvi and S. Chattopadhyay, *Appl. Water Sci.*, 2017, **7**, 3041–3054.

47 I. Langmuir, *J. Am. Chem. Soc.*, 1918, **40**, 1361–1403.

48 H. Freundlich, *J. Am. Chem. Soc.*, 1906, **62**, 21–125.

49 R. Sips, *J. Chem. Phys.*, 1948, **16**, 490–495.

50 A. L. Srivastav, P. K. Singh, V. Srivastava and Y. C. Sharma, *J. Hazard. Mater.*, 2013, **263**, 342–352.

51 W. Konicki, M. Aleksandrzak, D. Moszyński and E. Mijowska, *J. Colloid Interface Sci.*, 2017, **496**, 188–200.

52 M. Antônio, P. Kelm, M. José, S. Henrique, D. B. Holanda, C. Maria, B. De Araujo, R. Barbosa, D. A. Filho and E. J. Freitas, *Environ. Sci. Pollut. Res.*, 2019, **26**, 28558–28573.

53 Y. Liu, X. Zhao, J. Li, D. Ma and R. Han, *Desalin. Water Treat.*, 2012, **46**, 115–123.

54 G. Zhang, J. Qu, H. Liu, A. T. Cooper and R. Wu, *Chemosphere*, 2007, **68**, 1058–1066.

55 M. Vakili, S. Deng, L. Shen, D. Shan, D. Liu and G. Yu, *Sep. Purif. Rev.*, 2019, **48**, 1–13.

56 J. Lu, F. Fu, L. Zhang and B. Tang, *Chem. Eng. J.*, 2018, **346**, 590–599.

57 J. Kim and S. Hyun, *Sci. Total Environ.*, 2018, **615**, 805–813.

58 L. Yan, Y. Liu, Y. Zhang, S. Liu, C. Wang, W. Chen, C. Liu, Z. Chen and Y. Zhang, *Bioresour. Technol.*, 2020, **297**, 122381–122391.

59 Y. Dai, K. Zhang, X. Meng, J. Li, X. Guan, Q. Sun, Y. Sun, W. Wang, M. Lin, M. Liu, S. Yang, Y. Chen, F. Gao, X. Zhang and Z. Liu, *Chemosphere*, 2019, **215**, 163–172.

60 S. Bhatia and N. Verma, *Mater. Res. Bull.*, 2017, **95**, 468–476.

61 A. M. Puziy, O. I. Poddubnaya, R. P. Socha, J. Gurgul and M. Wisniewski, *Carbon*, 2008, **46**, 2113–2123.

62 R. C. Pereira, M. C. Arbestain, M. V. Sueiro and J. A. Maciá-Agulló, *Soil Res.*, 2015, **53**, 753–762.

63 Q. Fan, J. Sun, L. Chu, L. Cui, G. Quan, J. Yan, Q. Hussain and M. Iqbal, *Chemosphere*, 2018, **207**, 33–44.